Oil Shale, 2023, Vol. 40, No. 2, pp. 151–165
doi: https://doi.org/10.3176/oil.2023.2.04
ISSN 0208-189X


# Mass and heat transfer to and from oil shale exposed to a gas stream at constant temperature

Carla Cristina Moratori*, Antonio Carlos Luz Lisbôa

School of Chemical Engineering, University of Campinas, São Paulo, Brazil

Received 13 December 2022, accepted 14 April 2023, available online 10 May 2023

***Abstract.*** *The Irati Formation located in Southern Brazil is the world's second largest resource of oil shale from which shale oil has been produced by Petrobras, a Brazilian state-owned oil company, by the Petrosix® process. The shale plant was sold to a private company in November 2022. This study analyses the mass and heat transfer between oil shale particles and a gas medium by mathematical modelling using Fortran programs, focusing on the temperature and moisture gradients within the shale particles. It also carries out parametric sensitivity analysis regarding shale thermal conductivity, heat transfer coefficient, effective mass diffusivity, shale density and size. The particle size and effective mass diffusivity have a great impact on heat and mass transfer.*

***Keywords:*** *oil shale, mass transfer, heat transfer, pyrolysis, mathematical modelling.*

## 1. Introduction

Due to its versatility and availability, petroleum became responsible for about 39% of all energy consumed in the world [1]. Besides being used as fuel in engines and furnaces, it is widely consumed as a source of essential materials such as plastics and fibers.

In spite of all the advantages of renewable energy resources, the near future demand of energy will not be matched by them. It is understood that only by 2050 the renewable sources of energy will level up to fossil fuel. Meanwhile the petroleum market will continue to grow to face the demands of energy, mostly from developing countries [2].

At the same time, society will search for alternative energies such as solar, geothermal, hydroelectric and wind, as well as oil sands, coal and natural gas.

* Corresponding author: e-mail *ccmoratori@gmail.com*

Shale, due to its abundance, is a concrete possibility. The interest in oil shale to produce shale oil grew during the oil shocks in the 1970s. Its commercial use in the 1980s dwindled with the subsequent stability of the petroleum availability and price. Nonetheless the interest in shale rose again in the 21th century, mostly due to uncertainties in the petroleum market [3, 4].

In spite of the industrial use of shale along many years, most of its extraction technology was developed empirically. Even being an industry older than that of petroleum, the engineering of shale processing is less developed, and still poses a great challenge. The mechanism of breaking by pyrolysis the enormous molecules of solid kerogen – the organic matter scattered throughout shale – and subsequently breaking the bitumen produced into oil and gas continuously deserves more investigation.

The organic matter, named kerogen, is pyrolyzed upon heating to temperatures above 350 °C, releasing oil and gas. The oil may be refined to produce similar derivatives to petroleum ones, therefore constituting an alternative energy source. The gas may be used as fuel in the retorting plant; furthermore, due to its low sulphur content, it may be used in the ceramic industry, in which flue gas is in direct contact with raw material.

Brazil has had a strategic interest towards shale, for the country owns the second largest resource of it. The deposits are located in the States of Bahia, Ceará, Maranhão, Paraná, Rio Grande do Sul, Santa Catarina, São Paulo, Goiás and Amapá [5]. The most promising deposit is in the Irati Formation, which extends throughout the Southern region.

The company in charge of processing shale in Brazil is Petrobras, a state-owned oil company, which has a production unit in São Mateus do Sul, Paraná. A 64 t/h shale prototype unit started operation in 1972 and was definitely shutdown after 40 years of operation. It was followed by an industrial scale unit, 260 t/h, crowning the Petrosix® process. This process employs a moving bed retort, 34 m high and 11 m in diameter. The prototype unit was 5.5 m in diameter; it is the one considered in this investigation.

In 2020 the amount of raw shale processed in Brazil was 1.6 million tons, about 8% more than the previous year [6].

There are many other shale retorting technologies, mostly developed in the USA and China, some in situ and some aboveground [3]. Shales may be widely different, according to the type of sediment that gave origin to them. Therefore, their physical and chemical properties are unique. As such, each one may have a more adequate mean to be processed.

As the industrial processing has been developed mostly empirically, the understanding of pertinent phenomena is helpful to learn about the best conditions to produce shale oil [7].

## 2. Materials and methods

The first mathematical model, expressed by Equation (1), describes the temperature within the shale particles ($T_x$) when in contact with a gas stream at a constant temperature ($T_g$). In the actual retorting process, both vary with position.

The gas physical properties are calculated by equations provided in the literature [8, 9].

The origin of the cartesian coordinate system (point 0,0,0) is located in the center of the particle, as shown in Figure 1.

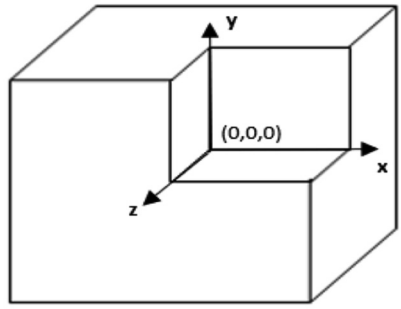


Fig. 1. Representation of a shale particle, considering a cartesian system. The origin of the axes is placed in the middle of the particle [10].

Equation (1) describes the temperature of the particle as a function of the position within the particle and time:

$$\frac{\partial T_x}{\partial t} = \alpha \cdot \left( \frac{\partial^2 T_x}{\partial x^2} + \frac{\partial^2 T_x}{\partial y^2} + \frac{\partial^2 T_x}{\partial z^2} \right), \tag{1}$$

where $\alpha = \frac{k_x}{\rho_x c_x}$ is the shale thermal diffusivity; $k_x$ is the shale thermal conductivity; $\rho_x$ is the shale density and $c_x$ is the shale heat capacity.

This equation regards the temperature as a function of the shale diffusivity $\alpha$ and considers the possibility of a temperature gradient along each axis of the cartesian system. The boundary conditions are described by Equations (2)–(8):

$$x = 0 \qquad \frac{\partial T_x}{\partial x} = 0, \tag{2}$$

$$x = \frac{L_1}{2} \qquad -k_x \cdot \frac{\partial T_x}{\partial x} = h \cdot \left( T_x - T_g \right), \tag{3}$$

$$y = 0 \qquad \frac{\partial T_x}{\partial y} = 0, \tag{4}$$

$$y = \frac{L_2}{2} \qquad -k_x \cdot \frac{\partial T_x}{\partial y} = h \cdot \left(T_x - T_g\right), \tag{5}$$

$$z = 0 \qquad \frac{\partial T_x}{\partial z} = 0, \tag{6}$$

$$z = \frac{L_3}{2} \qquad -k_x \cdot \frac{\partial T_x}{\partial z} = h \cdot \left(T_x - T_g\right), \tag{7}$$

$$t = 0 \qquad T_x = T_{xe}. \tag{8}$$

At the surfaces, boundary conditions of third type, Equations (3), (5) and (7), are considered.

The heat transfer coefficient is calculated by Equation (9) for packed beds [11]:

$$Nu = \frac{h \cdot d_p}{k_g} = 2 + 1{,}8 \cdot Re^{\frac{1}{2}} \cdot Pr^{\frac{1}{3}}, \tag{9}$$

where $Nu$ is the Nusselt number, $Re$ is the Reynolds number, $Pr$ is the Prandtl number, $d_p$ is the particle diameter and $k_g$ is the gas thermal conductivity.

Another mathematical model describes the moisture content ($U_x$) profile within the particle, when in contact with a gas stream. The most relevant parameter is the shale effective diffusivity, obtained by Porto [12].

According to Perazzini [13], the effective diffusivity of moisture in porous media is an average value of all existing diffusive mechanisms, taking into account properties of the solid matrix and the pore.

To describe the moisture profile within the particle, the same particle representation (Fig. 1) was employed, with the same coordinate system.

The initial moisture content ($U_{xe}$) is 4 % (mass).

This value is the one existing in the shale from the Irati Formation.

The partial differential Equation (PDE) (10) describes the moisture content as a function of position and time:

$$\frac{\partial U_x}{\partial t} = D_{eff} \cdot \left(\frac{\partial^2 U_x}{\partial x^2} + \frac{\partial^2 U_x}{\partial y^2} + \frac{\partial^2 U_x}{\partial z^2}\right). \tag{10}$$

The moisture content is a function of the effective diffusivity ($D_{eff}$) which acts in all directions. The boundary conditions are given by Equations (11) to (14). A boundary condition of type 2 was considered at the surfaces, for once the moisture reaches the particle surfaces, it is immediately dragged by the water vapour stream – most of the gas stream in the Petrosix process is steam:

$$x = 0 \text{ and } x = \frac{L_1}{2} \qquad \frac{\partial U_x}{\partial x} = 0, \tag{11}$$

$$y = 0 \text{ and } y = \frac{L_2}{2} \qquad \frac{\partial U_x}{\partial y} = 0, \tag{12}$$

$$z = 0 \text{ and } z = \frac{L_3}{2} \qquad \frac{\partial U_x}{\partial z} = 0, \tag{13}$$

$$t = 0 \quad / \quad U_x = U_{xe}. \tag{14}$$

The numerical solution of PDEs was reached by discretization of the special dimensions using finite differences. PDEs were applied to each point of a grid within the particle, forming a set of ordinary differential equations (ODE). The Numerical Method of Lines was employed as described by Schiesser [14, 15].

The set of ODEs was then solved by the Runge-Kutta-Fehlberg method.

## 3. Results and discussion

### 3.1. Dimension

The particle size is a major parameter in the heat and mass transfer involving shale and gas. A few particle dimensions were investigated. Figure 2 shows a typical particle obtained from the feedstock of the Petrosix® process. Its dimensions determined the top limits of the particle sizes of this investigation.

Fig. 2. Raw shale particle of Petrosix® process.

The Table presents three dimensions of shale particles.

**Table. Dimensions of shale particle**

| Particle | % | Length, cm | Height, cm | Depth, cm |
|---|---|---|---|---|
| P1 | 130 | 14 | 7 | 4 |
| P2 | 100 | 11 | 5 | 3 |
| P3 | 70 | 8 | 4 | 2 |

The particle (P1) shown in Figure 2 is the largest. The particle (P2) with an axis roughly 30% smaller was examined in this study. The smallest particle (P3) had an axis approximately 30% smaller than that of (P2). The volume of the biggest particle (P1) is 237% larger than the (P2) volume, while the volume of the smallest (P3) is 39% of (P2)'s.

Figure 3 exhibits temperature profiles of the center (C) and surface (S) of each particle (a) and their temperature difference between the surface and the center (b). A gas temperature of 400 °C and a residence time of 90 min were considered.

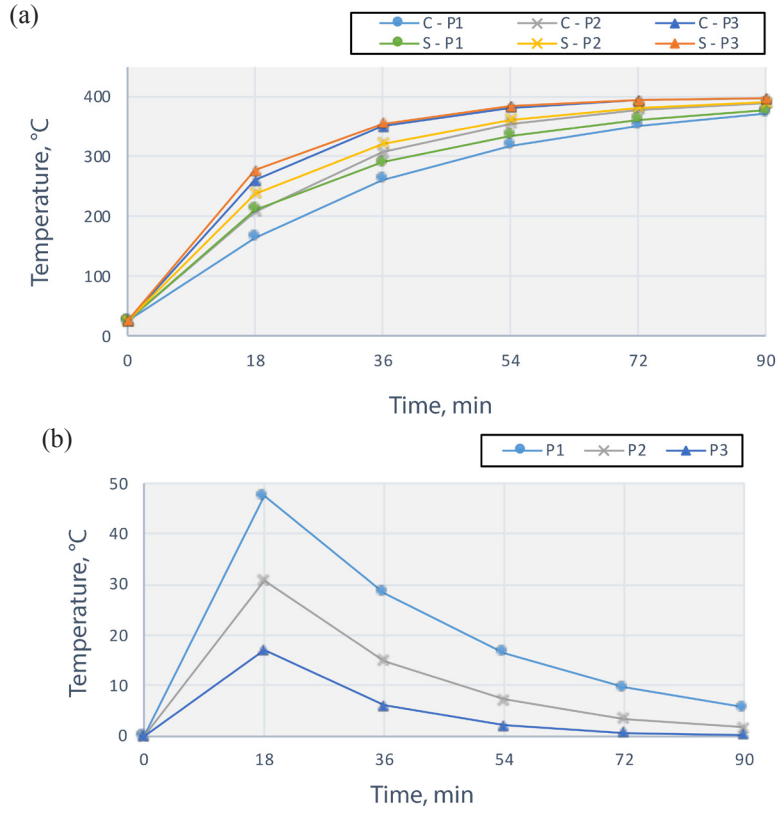


Fig. 3. Temperature profiles of center and surface points (a) and respective differences for shale particles (b) with different dimensions.

As seen from Figure 3, the temperature differences from the surface and the center are the largest for the bigger particles and decline with time, as all temperatures tend to decrease to the gas one.

Figure 4 displays moisture profiles of the center and near surface of each particle (a) and their moisture difference between the center and the near surface (b).

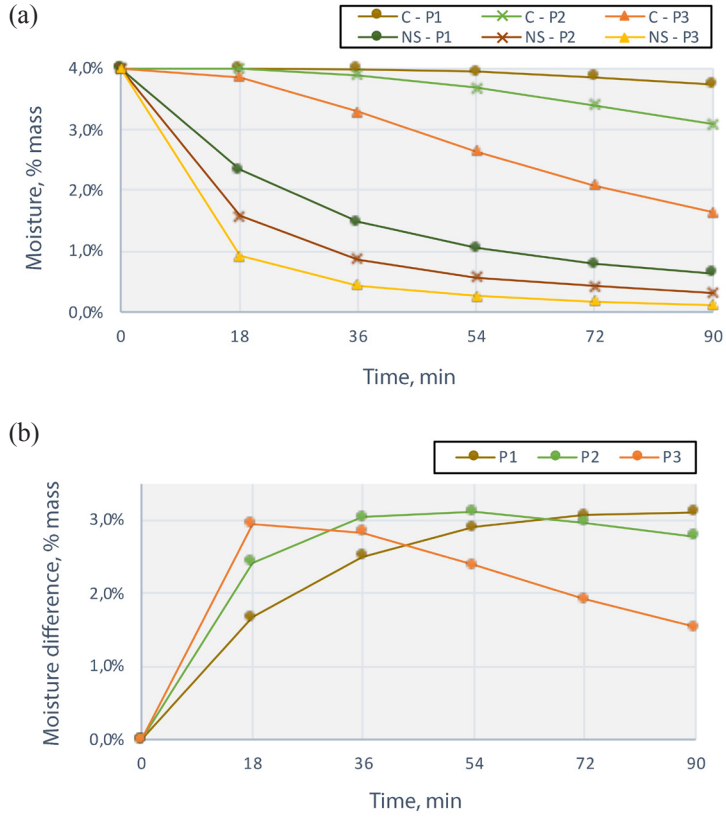


Fig. 4. Moisture profiles of center and near surface points (a) and respective differences for shale particles (b) with different dimensions.

Figure 4 indicates that at 18 minutes, the smaller particles have a moisture content difference of 3.0% (mass) between the particle center and near surface and the largest difference, 1.7%. At 90 minutes, the differences alter to 1.5% and 3.1%, respectively.

In addition, Figure 4 reveals that the smaller particles lose moisture faster. During the period considered, the center of the largest particle almost did not lose any moisture (3.7%), while in the smallest one the content dropped to half (1.6%). As to the moisture difference between the center and the near surface, the largest particle had initially the smallest values, which increased with time, as expected. The smaller the particle, the faster the drying process throughout the particle.

### 3.2. Heat transfer coefficient

Figure 5 exhibits temperature profiles of the center and surface of each particle (a) and their temperature differences between the center and the surface (b) as a function of heat transfer coefficient. This coefficient is calculated in each iteration by Equation (9).

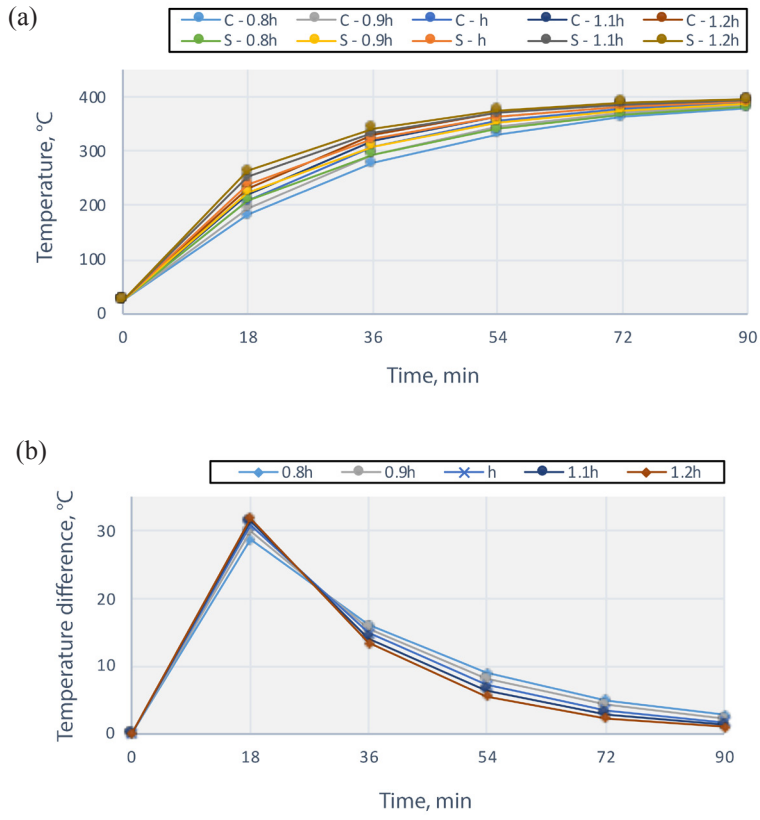


Fig. 5. Temperature profiles of center and surface points (a) and respective differences for shale particles (b) at different heat transfer coefficients.

It can be seen from Figure 5 that the temperature differences are higher in the beginning of heat transfer but become smaller with time. At 18 minutes, the differences are between 28.7 and 31.7 °C; at 90 minutes, they are 2.8 and 1.0 °C for the lower and higher heat transfer coefficient, respectively. The temperature differences between the vertices and the center are inversely proportional to the heat transfer coefficient. The differences are slightly higher with lower coefficients but are reduced with time. The higher the heat transfer coefficient, the higher the temperature within the particles, as expected.

### 3.3. Shale thermal conductivity

Figure 6 depicts temperature profiles of the center and surface of each particle (a) and their temperature differences between the center and the surface (b) as a function of shale thermal conductivity. According to Schön [16], the shale thermal conductivity is 3.84 W $m^{-1}$ $K^{-1}$.

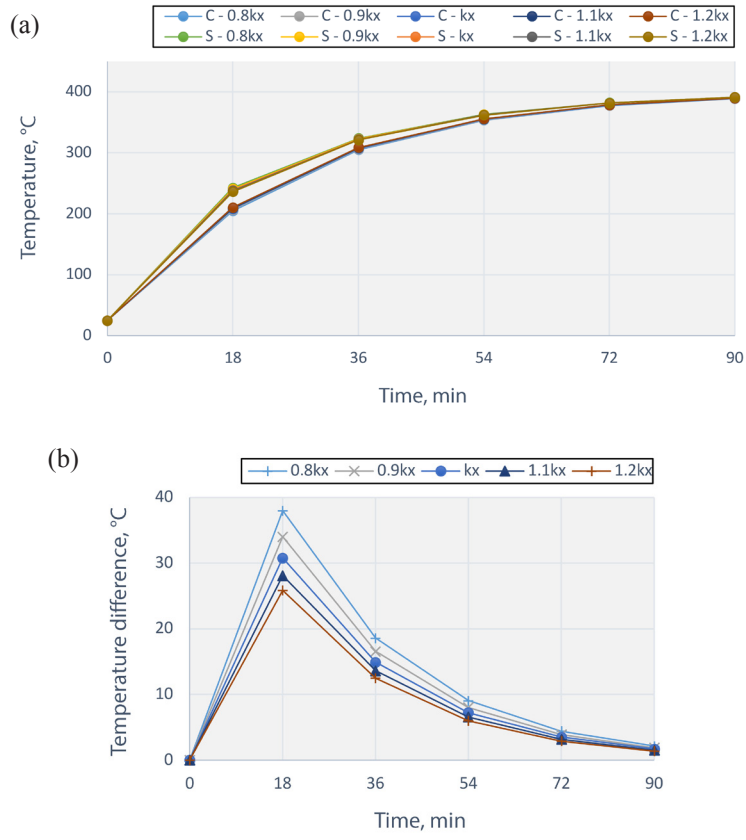


Fig. 6. Temperature profiles of center and surface points (a) and respective differences for shale particles (b) at different shale thermal conductivities.

The impact of changing the thermal conductivity value on heat balance is almost unnoticeable, as seen from Figure 6.

At 18 minutes, the temperature difference between the particle vertices and center is 38.0 °C and 25.8 °C for the lowest ($0.8*k_x$) and the highest ($1.2*k_x$) thermal conductivity value, respectively. At 90 minutes, these differences come down to 2.1 °C and 1.4 °C for the lowest and the highest value, respectively.

The temperature differences between the extreme points are inversely proportional to the thermal conductivity. The differences are higher at lower

conductivities, which diminish with time. The temperatures are slightly higher with higher thermal conductivities. The lower the thermal conductivity, the lower the temperatures and the higher the differences between the particle vertices and center.

### 3.4. Shale heat capacity

Figure 7 shows temperature profiles of the center and surface of each particle (a) and their temperature differences between the center and the surface (b) as a function of shale heat capacity. The shale heat capacity is 1247.7 J $kg^{-1}$ $°C^{-1}$, based on the raw shale temperature of 300 °C [17]. As the equations developed by Lee [17] do not consider the range from room temperature to pyrolysis temperature, 300 °C is adopted as an intermediate temperature.

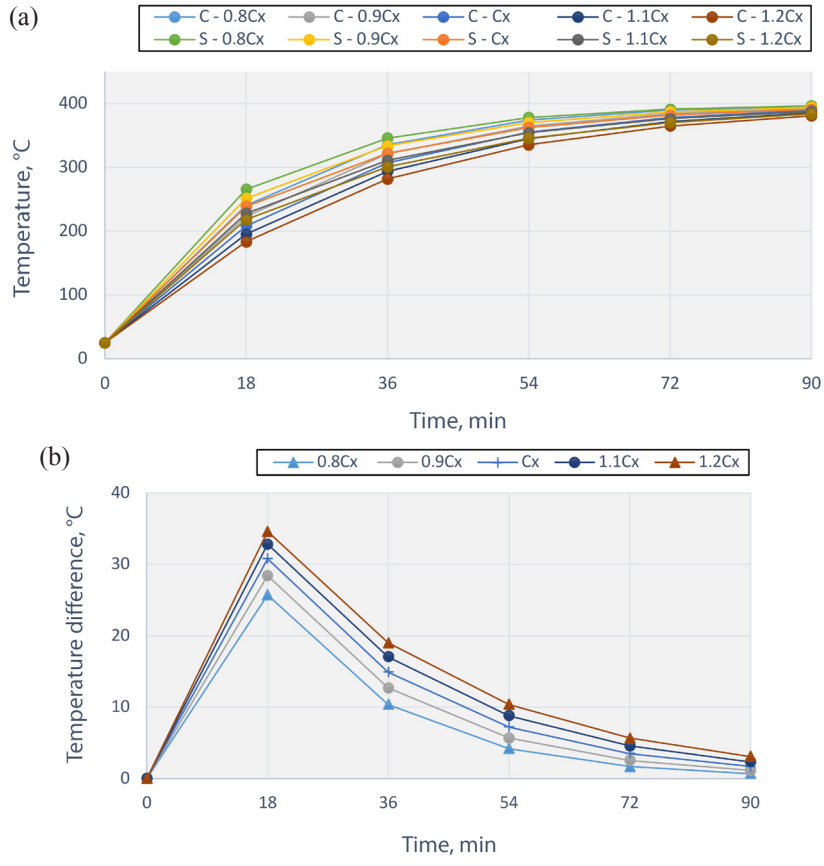


Fig. 7. Temperature profiles of center and surface points (a) and respective differences for shale particles (b) at different shale heat capacities.

Figure 7 indicates how the shale heat capacity impacts the heat balance. As before, the temperature differences between the particle vertices and center become smaller with time. The surface temperature and that of gas are also reduced.

The temperature differences are directly proportional to those of heat capacity. These differences are slightly higher for higher heat capacities and the temperatures possess lower values.

At 18 minutes and 90 minutes, the particle temperatures between the vertices and the center are 25.7 ℃ and 0.7 ℃ for the lower heat capacity ($0.8*C_x$) and 34.6 ℃ and 3.1 ℃ for the highest heat capacity ($1.2*C_x$), respectively.

The temperature differences between the surface and the center of the particles arise because the higher the heat capacity, the greater the energy necessary to increase the temperature. For the same reason, the temperature difference between the shale and the gas increases with shale heat capacity.

### 3.5. Shale density

Figure 8 displays temperature profiles of the center and surface of each particle (a) and their temperature differences between the center and the surface (b) as a function of shale density. The shale density is 2100 kg $m^{-3}$ [10].

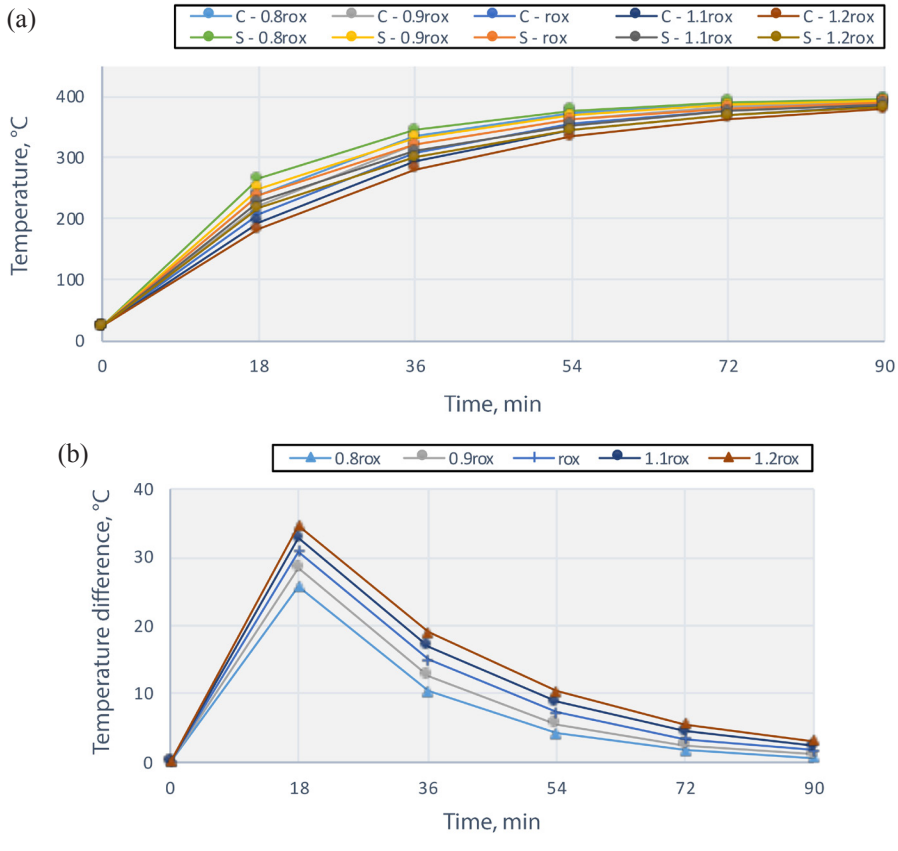


Fig. 8. Temperature profiles of center and surface points (a) and respective differences for shale particles (b) at different shale densities.

Shale density affects the heating process in the same way as heat capacity, as shown in Figure 7 and Figure 8. Both parameters are part of the effective thermal diffusivity denominator.

### 3.6. Effective mass diffusivity

Figure 9 exhibits moisture profiles at the center and near surface of each particle (a) and their moisture differences between the center and the near surface (b) as a function of effective mass diffusivity. The effective mass diffusivity is $8.10^{-9}$ m²/s [12].

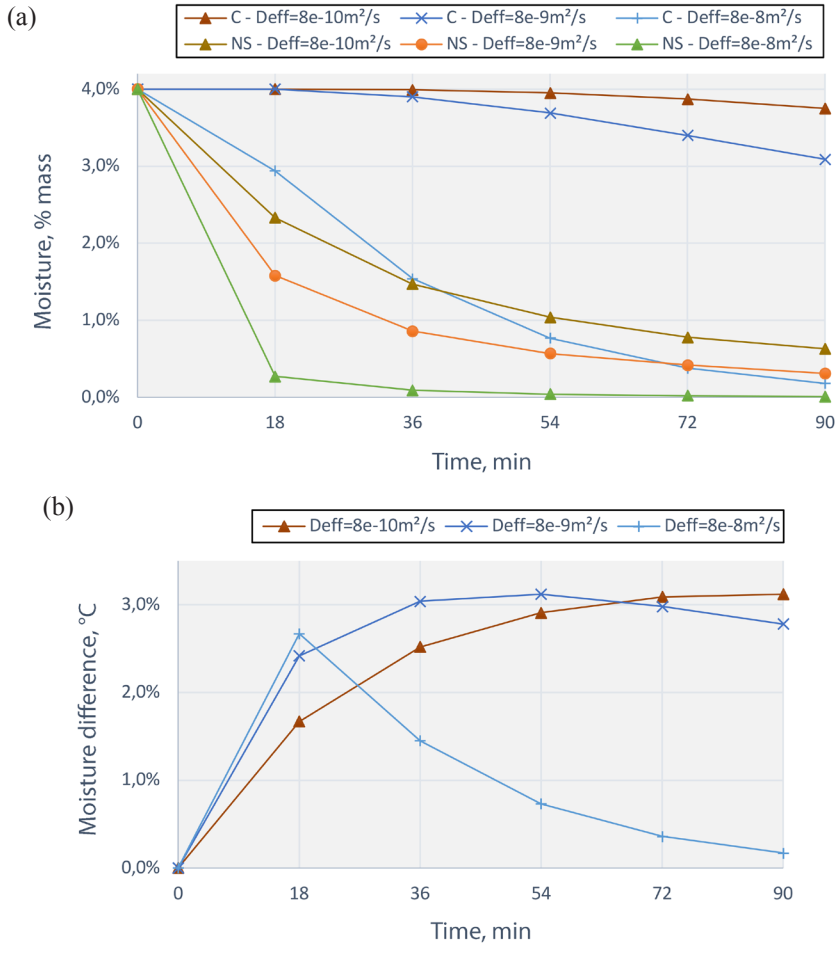


Fig. 9. Moisture profiles at the center and near surface points (a) and respective differences for shale particles (b) at different effective mass diffusivities.

In order to study the effect of this parameter in the drying process, effective mass diffusivity values had to be varied widely, to produce noticeable effects.

Similarly to what happens with the change in dimensions (Section 3.1), the changes in the diffusivity do not show a definite pattern in regard to differences in moisture content between the particle center and its near surface.

At the same time, at 18 minutes, for the lowest diffusivity, the moisture difference between the center and the near surface is 1.7%, being 2.7% for the highest diffusivity value. At 90 minutes, the moisture contents are 3.8% for the lowest diffusivity and 0.2% for the highest, as expected.

## 4. Conclusions

The models, developed in Fortran language, describing the temperature and moisture content, allow us to obtain the profiles of temperature and moisture content within the oil shale particles, providing a good insight of the effects of the shale properties in the heat and mass transfer in the retort.

The three-dimensional grid placed inside each particle provided the nods in which the heat and mass balances partial differential equations were applied. The largest particles have lower temperature profiles and higher moisture content profiles.

Regarding the difference between the particle surface temperature and its center temperature, the largest particles exhibit higher gradients than smaller particles.

Smaller particles are heated faster, consuming more energy from the gas, which cools faster.

There is no definite pattern regarding the moisture content difference between the particle near surface and its center. Although a small particle exhibits a larger concentration gradient initially, the moisture is quickly withdrawn, reducing the gradient.

The model solution indicates that the temperature difference between the particle surface and its center is inversely proportional to the heat transfer coefficient, while the temperature is proportional to it.

The difference between the particle surface and its center is inversely proportional to the thermal conductivity. A lower value of this parameter indicates a poorer capacity of heat transfer within the particle, causing larger gradients and lower temperatures. It was noticed that this parameter is the one which less affected the heat balances.

As to the shale specific heat, it affects directly the difference between the center temperature and the surface temperature. A higher specific heat would produce a larger temperature gradient within the shale.

The effect of varying the effective diffusivity on the moisture transfer is not definite. For a low value of this parameter, moisture faces more difficulty to reach the surface, causing an increase with time of the difference between

the moisture content at the center and the near surface. An opposite behavior is encountered for the higher values of this parameter.

It was observed that the shale did not dry out within the time considered (90 min) when a suggested effective diffusivity is used. When increasing the period 10 times, the moisture content in the particle center reaches 0.18 % at the end of this time. In a retorting process the moisture initially present should be released to not compete with the pyrolysis energy demand.

## Acknowledgement

The publication costs of this article were partially covered by the Estonian Academy of Sciences.

## REFERENCES

1. IEA (International Energy Agency). *World Energy Outlook 2022*. United States, 2022.
2. EIA (U.S. Energy Information Administration). *International Energy Outlook 2021*. United States, 2021.
3. *Handbook of Alternative Fuel Technologies* (Lee, S., Speight, J. G., Loyalka, S. K., eds.). CRC Press, United States, Florida, 2007, 225–294.
4. National Geographic. *Oil Shale.* https://education.nationalgeographic.org/resource/oil-shale (acessed 2022-11-25).
5. Abreu, S. F. *Brazilian Mineral Resources*, Volume 2, 2nd Edition. São Paulo: Edgard Blücher, 1973 (in Portuguese).
6. ANP – Agência Nacional do Petróleo, Gás Natural e Biocombustíveis. *The Oil, Natural Gas and Biofuels Statistical Yearbook 2021*. Rio de Janeiro, 2021 (in Portuguese).
7. Almeida, A. R. F. *Investigation on the Mechanism of Oil Shale Desvolatilization*. MSc Dissertation. UNICAMP, Faculdade de Engenharia Química, 2005 (in Portuguese).
8. Moratori, C. C. *Heat Transfer on the Heating Zone of an Oil Shale Moving Bed.* MSc Dissertation. UNICAMP, Faculdade de Engenharia Química, 2014 (in Portuguese).
9. Matos, M. A. A. *Thermophysical Properties of Some Gases, Solids and Liquids.* Relatório Técnico. Departamento de Ambiente e Ordenamento, Universidade de Aveiro, Aveiro, Portugal, 1998 (in Portuguese).
10. Lisboa, A. C. L. *Investigations on Oil Shale Particle Reactions*. PhD Thesis. The Faculty of Graduate Studies Chemical and Bio-Resource Engineering, University of British Columbia, Vancouver, Canada, 1997.
11. Levenspiel, O. *Chemical Reaction Engineering*. 3rd Edition. John Wiley & Sons, New York, 1998.

12. Porto, P. S. S. *Investigation on Drying of Oil Shale Particles*. PhD Thesis. UNICAMP, Faculdade de Engenharia Química, 2005 (in Portuguese).
13. Perazzini, H. *Drying of Porous Granular Solids.* PhD Thesis. Centro de Ciências Exatas e de Tecnologia, Departamento de Engenharia Química, Universidade Federal de São Carlos, 2014 (in Portuguese).
14. Schiesser, W. E. *The Numerical Method of Lines: Integration of Partial Differential Equations*. Academic Press, 1991.
15. Schiesser, W. E. *Computational Mathematics in Engineering and Applied Science: ODEs, DAEs and PDEs*. CRC Press, Boca Ranton, 1994.
16. Schön, J. H. *Physical Properties of Rocks: Fundamentals and Principles of Petrophysics*. Pergamon, 1996.
17. Lee, L. M. *Specific Heat Determination of Oil Shale from the Irati Formation and from New Brunswick by Differential Scanning Calorimetry DSC-50.* MSc Dissertation. UNICAMP, Faculdade de Engenharia Química, 2001 (in Portuguese).